Available online at www.sciencedirect.com
SCIENCE DIRECT
ELSEVIER
Ocean Engineering 32 (2005) 1829–1840
OCEAN ENGINEERING
www.elsevier.com/locate/oceaneng

Distributions of void fraction under breaking waves in the surf zone

Ashabul Hoque[a,*], Shin-ichi Aoki[b]

[a]*Department of Mathematics, University of Rajshahi, Rajshahi 6205, Bangladesh*
[b]*Department of Architecture and Civil Engineering, Toyohashi University of Technology, Toyohashi 441-8580, Japan*

Received 20 August 2004; accepted 19 November 2004
Available online 1 April 2005

Abstract

Void fractions under breaking waves have been measured by a conductivity probe. Empirical coefficients k_0 and C_0 have been determined through the experimental results and found to be function of the local wave height and relative distance, respectively. The results indicate that the distributions of void fraction follow closely analytical solution of the diffusion equation.

Keywords: Void fraction; Surf zone; Breaking waves; Diffusion equation

1. Introduction

The rate of air bubble transport is needed for various purposes such as the gas exchanges, wave energy transferred, sediment transport and sound generation (e.g. Koga, 1982; Wu, 1988; Lamarre and Melville, 1991; Waniewski et al., 2001). In shallow water, the sloping bottom causes the breaking process, where a large amount of air bubble entrains into water near the breaking point. With the mixing of air bubbles, the flow fields of broken waves are turbulent and complicated. The injected air bubbles beneath a breaking wave are rapidly broken up by turbulence, producing an initial size spectrum proportional to $(\text{radius})^{-10/3}$ (Garrett et al., 2000). This tiny air bubbles are not always visible to the naked eye, yet they play a very important role in the surf zone.

* Corresponding author.
E-mail addresses: ashabulh@yahoo.com (A. Hoque), aoki@jughead.tutrp.tut.ac.jp (S.-i. Aoki).

0029-8018/$ - see front matter © 2005 Elsevier Ltd. All rights reserved.
doi:10.1016/j.oceaneng.2004.11.013

Studies on surf zone air bubbles are very limited yet, probably because the flow fields of broken wave are very complicated after mixing the air bubbles. It is almost unclear how these air bubbles affect the fluid motion in the surf zone. Only a small number of studies investigated the characteristics of surf zone air bubbles. Chanson et al. (2002) showed that the air entrainment process and bubble residence time are affected by the sloping bottom. The entrained bubbles induce a rise in water level associated with an energy transfer into potential energy while breaker-generated waves propagate in off and onshore directions (e.g. Führböter, 1970; Hwung et al., 1992). Loewen and Melville (1994) showed that the presence of air bubbles in the surface layer, the compressibility of the mixture is increased, and therefore, the speed of sound is reduced.

The study concentrates on shoaling of unidirectional regular waves that includes spilling and plunging type of breaking. For plunging breakers, the entrainment of air bubbles is caused by the top of the wave forming a water jet projecting ahead of the wave face and entraining air when it impacts the water free surface in front of the wave (e.g. Chanson and Lee, 1997). With spilling breakers, the air bubbles travel with the wave as a surface roller and finally entrains into water. In both cases, air bubble entrainment is still significant (Fig. 1).

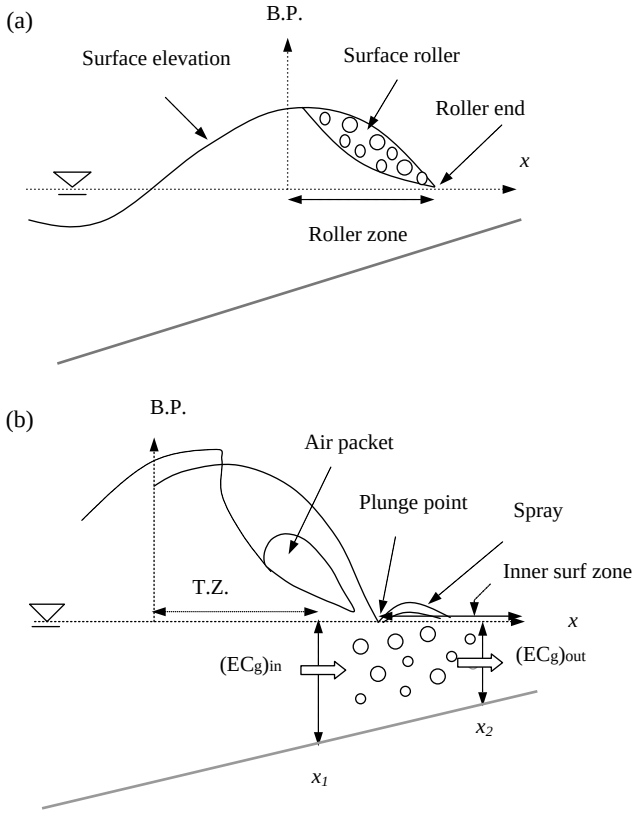

Fig. 1. Breaking waves. (a) Sketch of a spilling breaker; (b) sketch of a plunging breaker.

The complex two-phase flow arising from breaking has made theoretical and experimental progress. In this paper, we describe a device capable of measuring the void fraction (volume fraction of air) in the surf zone.

2. Experiments

2.1. Instrumentation

Two typical waves breaking were generated in a wave channel of 20 m long, 0.80 m wide, and 0.60 m deep. The bed slope of wave flume was 1/9.5. Experiments were conducted with tap water and ambient air and the experimental conditions are tabulated in Table 1.

The effect of air bubbles on wave gauge and displacement meter reading was tested in a preliminary experiment. Air was introduced at the bottom end of a vertical cylinder installed in a still water tank. Visual observations showed that the foam was confined to a region above the still water level. Tests, performed with void fractions ranging from 0 to 0.10, showed that both wave gauges and displacement meter recorded with a reasonable accuracy the rise in water level induced by the air bubbles. The error was of the same order of magnitude as the bubbly foam thickness formed at the water surface in the cylinder, although the output of the gauge tended to correspond to the level above the foam (Fig. 2). Fig. 2 presents measured super elevations above still water as functions of the depth-average void fraction for comparable tests.

The L-shape conductivity probe was used for two-dimensional wave breaking. The effect of air bubbles on the wave gauge was tested in separate experiments. The probe, wave gauges and pointer gauge were fixed on a trolley system and displaced in the horizontal and vertical directions. The probe tip was set up in the opposite direction of wave propagation and void fraction was measured with a grid spacing of 5–25 cm increment along channel and 2 cm increment in the depth.

2.2. Wave generation

A wave breaks as it approaches the shore is a function of how steep the wave is and how gently the beach slopes. Iribarren and Nogales (1949) used the parameter, which called

Table 1
Wave breaking experiments: characteristics of wave breaking

Test (1)	H_0 (m) (2)	T (s) (3)	H_0/L_0 (4)	H_b (m) (5)	H_b/h_b (6)	I_0 (7)	Br. type (8)
SP-1	0.110		0.056	0.117	1.08	0.443	
SP-2	0.122	1.12	0.062	0.133	1.03	0.421	Spilling
SP-3	0.150		0.076	0.149	0.91	0.380	
PL-1	0.125		0.024	0.180	1.01	0.677	
PL-2	0.145	1.80	0.028	0.198	1.05	0.627	Plunging
PL-3	0.166		0.032	0.207	1.07	0.586	

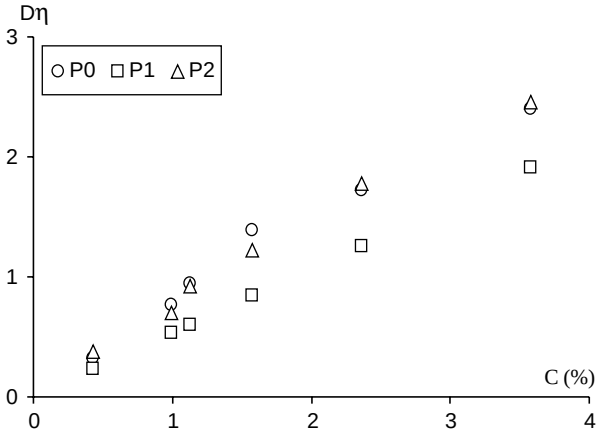

Fig. 2. Accuracy of capacitance water gauge and displacement meter in bubbly waters: superelevation as a function of the depth-averaged void fraction. Here P0, P1 and P2 represent the wave gauge, pointer gauge below foam and pointer gauge above foam, respectively.

the surf similarity parameter:

$$I_0 = \frac{m}{\sqrt{H_0/L_0}} \tag{1}$$

where, m represents the beach slope, H_0 and L_0 are the wave height and wavelength at deep water, respectively.

Detailed measurements were performed for three tests in both cases of spilling and plunging breakers. Galvin (1968) found that in general the Iribarren number I_0 can be related to the type of wave breaking in the range 0.45–3.2 for plunging waves and $I_0 < 0.45$ for spilling waves. A summary of the characteristics of waves breaking is given in Table 1.

2.3. Response of probe tip and data analysis

A sketch of air pulses and wave profile are shown in Fig. 3(a), which is used to determine the void fraction. When a bubble hits a probe tip, the output of the void meter rises like the region between 1 and 2 in Fig. 3(b). Region between 2 and 3 shows the tip is completely inside the bubble where the output is constant. As the tip touches the bubble-water surface again which is indicated by the region between 3 and 4, the response is much faster than the region between 1 and 2 due to surface tension.

In data processing for the output from the probe, negative voltage is set '0' that indicates water and the positive voltage set to '1' that indicates air. The outputs from the wave gauges were multiplied by the calibration coefficient to obtain elevation of water. In the duration of breaking event which the probe is immersed under water, Δt, the total time of air bubble encounter, $\Delta\tau$, is given as

$$\Delta t = \sum_{\Delta t} \Delta\tau_i \tag{2}$$

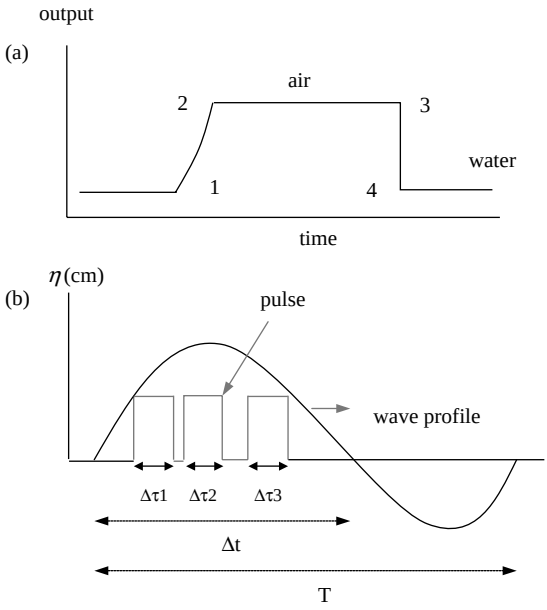

Fig. 3. Sketch. (a) Output signal from a probe during the passage of a bubble; (b) response of the wave gauge and probe.

where $\Delta\tau_i$ is the period that an air bubble takes when it passes the probe tip and i denotes a number of air bubbles detected during Δt.

The void fraction for one wave period T is obtained as

$$C = \frac{\sum_T \Delta\tau}{\sum_T \Delta t} \tag{3}$$

Figs. 4 and 5 present the measurements of time averaged void-fraction during one wave period for spilling and plunging breaker, respectively. Approximately 570 waves were extracted from 10 min data recording for each depth in spilling breaker, whereas it were 350–420 waves from 10 to 12 min data for plunging breaker. Finally, it was found the mean void fraction for each vertical depth from Figs. 4 and 5.

3. Analysis of the air bubble diffusion process

3.1. Vertical distribution of void fraction

The void fraction in a channel section is determined from its relation with a representative void fraction such as the mean void fraction on a vertical line in the section. It is a common practice to conduct depth-averaged sampling to directly determine the vertical mean void fraction. However, during high water and unsteady flow periods, strong currents make the depth-averaged sampling unpractical. In this situation, we can conduct

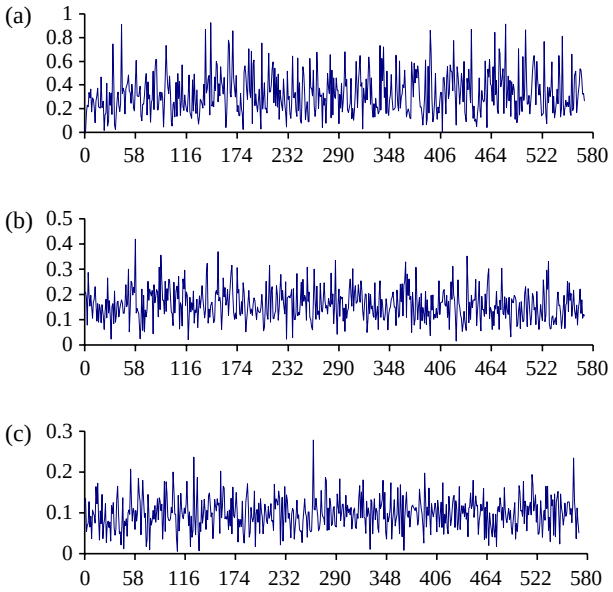

Fig. 4. Time averaged void fraction over one wave period versus number of waves measured at $x-x_b=0.50$ m ($H_0/L_0=0.076$: spilling breaker). (a) 2 cm above the still water level; (b) at still water level and (c) 2 cm below the still water level.

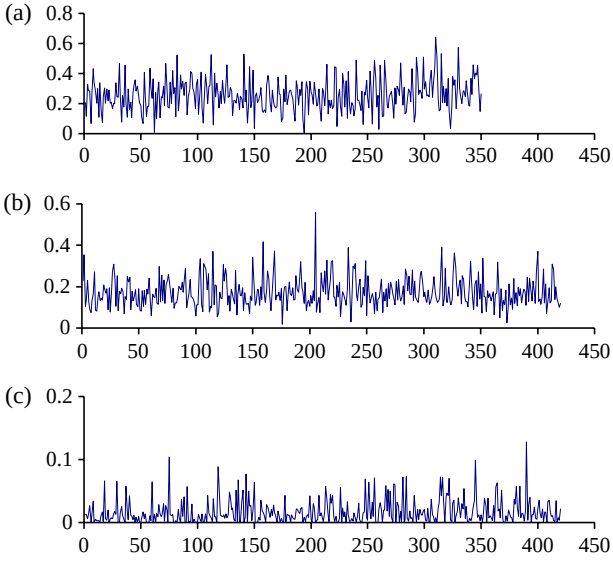

Fig. 5. Time averaged void fraction over one wave period versus number of waves measured at $x-x_b=0.70$ m ($H_0/L_0=0.024$: plunging breaker). (a) 2 cm above the still water level; (b) at still water level and (c) 4 cm below the still water level.

a point sampling and use a mathematical model to translate the single sample into the mean void fraction.

For a small control volume, the uniform steady flow for air in the air–water in term of the simplest differential equation governing on a vertical axis is

$$\frac{\partial}{\partial z}(CV) = \frac{\partial}{\partial z}\left(D_t \frac{\partial C}{\partial z}\right) \tag{4}$$

where C = void fraction at z, z = vertical distance measured from mean water surface $z=0$, and D_t denotes the turbulent diffusivity of air bubble in air–water.

Now assume velocity distribution is uniform and D_t is independent in the z-direction then, we have

$$\frac{\partial^2 C}{\partial z^2} = \frac{V_0}{D_t}\frac{\partial C}{\partial z} \tag{5}$$

where V_0 represents the uniform velocity. Therefore, solution of Eq. (5) gives

$$C(z) = C_0 \exp(k_1 z) \tag{6}$$

where $k_1 = V_0/D_t$ is a decay parameter characterizing vertical distribution of air bubbles and C_0 denotes the reference void fraction at the mean water surface $z=0$.

The following boundary conditions are automatically satisfied:

$$C(z) = C_0 \quad \text{at the surface } z = 0$$

and

$$C(z) \to 0 \quad \text{for } z \to -\infty$$

3.2. Determination of empirical coefficient k_1 and C_0

In Eq. (6), the unknown parameters are k_1 and C_0. The values of these parameters can be estimated by comparison with experimental data. Introducing a new dimensionless parameter k_0 is defined as

$$k_0 = k_1 H \tag{7}$$

where H is a local wave height.

The parameter k_1 for void fraction distribution in the surf zone was determined by fitting a theoretical curve to the experimental data for both spilling and plunging breakers. k_1 has smaller value when penetration is larger and vice-versa. It would be preferable to choose a single value for k_0, which gives satisfactory results for all cases, allowing the model to be used on beaches with arbitrary shape. As shown in Fig. 6, though k_0 varies a little with wave steepness and with the distance from the breaking point, it shows nearly constant value. Thus, Eq. (7) suggests that k_1 increases with decreasing H. It is found from the figures that $k_0 = 3.75$ for spilling breaker and $k_0 = 4$ for plunging breaker which are shown by the dashed lines.

On the other hand, to find a reasonable value or expression of C_0, three sets of data are used in Fig. 7 for both spilling and plunging breakers. The parameters C_0

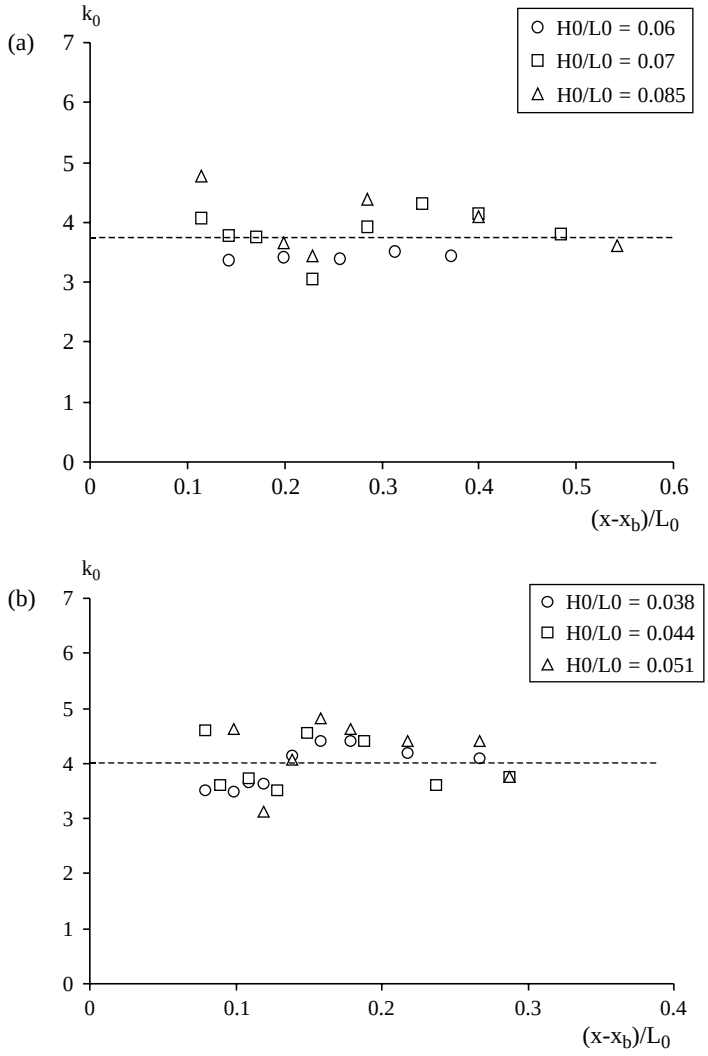

Fig. 6. Relationship between dimensionless parameter k_0 and distance. (a) Spilling breaker and (b) plunging breaker.

was calculated experimentally from the wave tests in the flume. The C_0 values exhibit in considerable scatter in both cases. The reason of this may be accurate measurement is not possible near the free surface due to strong turbulence. In Fig. 7, the best-fit curves to the values of C_0 are shown which depends on the horizontal distance from the breaking point $(x-x_b)/L_0$.

All the data for void fraction are corrected by the following expressions for spilling and plunging breakers, respectively:

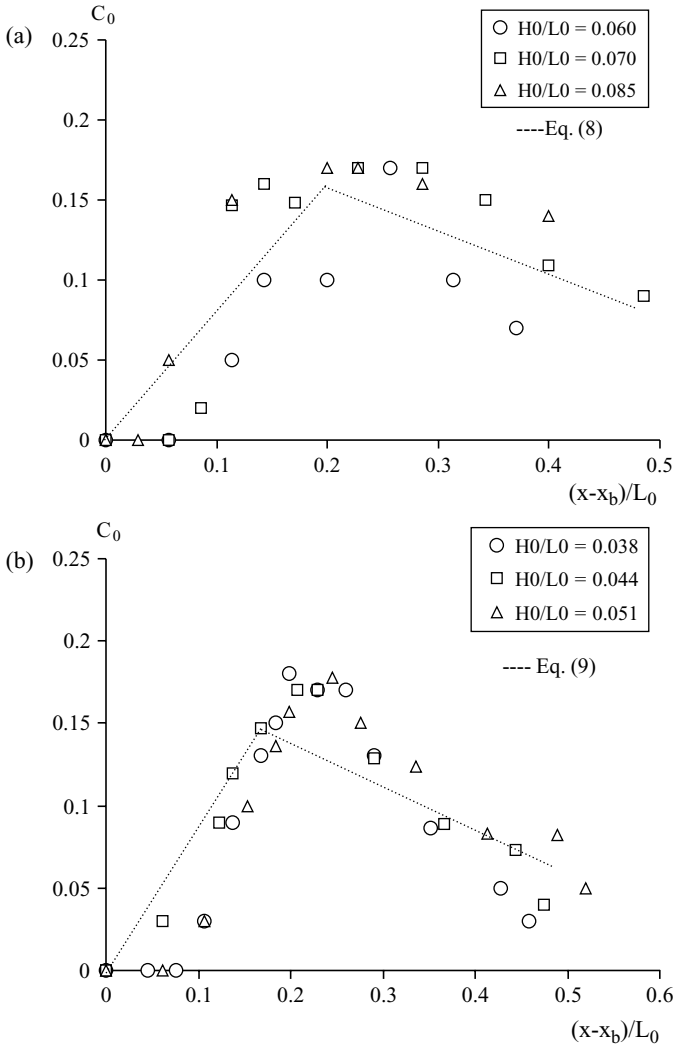

Fig. 7. Relationship between dimensionless parameter C_0 and distance. (a) Spilling breaker and (b) plunging breaker.

3.2.1. Spilling breaker

$$C_0 = 0.80\frac{(x-x_b)}{L_0} \quad \text{for } 0 \le \frac{(x-x_b)}{L_0} \le 0.20$$
$$C_0 = -0.39\frac{(x-x_b)}{L_0} + 0.238 \quad \text{for } 0.20 \le \frac{(x-x_b)}{L_0} \tag{8}$$

3.2.2. Plunging breaker

$$C_0 = 1.285\frac{(x-x_b)}{L_0} \quad \text{for } 0 \le \frac{(x-x_b)}{L_0} \le 0.14$$
$$C_0 = -0.75\frac{(x-x_b)}{L_0} + 0.285 \quad \text{for } 0.14 \le \frac{(x-x_b)}{L_0} \tag{9}$$

4. Results and discussion

Figs. 8 and 9 show the reliability of Eq. (6) in describing the vertical distribution of void fraction, in which the data used for comparison for both spilling and plunging breakers. In Figs. 8 and 9, the effect of k_0/H ($=k_1$) on void fraction distribution, in which several distributions are observed for each test of $H_0/L_0=0.076$ and $H_0/L_0=0.024$, respectively. This indicates that under a given set of wave conditions the void fraction distribution may vary section-to-section as the H may vary. In Fig. 8, the location $x-x_b=0.5$ m is identical with the end of roller (defined in Fig. 1(a)) and visual observation suggests that air bubbles penetrate maximum at this location. Fig. 8 also represents that the region between $x-x_b=$ 0.7 and 0.95 m corresponds to the inner surf zone (defined in Fig. 1(b)) and in this region, the results from the model agree well with the data.

On the other hand, in Fig. 9, the positions $x-x_b=0.6$ and 0.8 m are the plunge and plash up points, respectively. At the plunging point $x-x_b=0.6$ m, penetration depth becomes maximum. The measured results are affected just after the transition region (nearly $x-x_b=0.6$ m) due to turbulence, especially in plunging breakers and show a little disagreement near the still water surface.

In Figs. 8 and 9, we have seen that the data of void fraction consistently decays exponentially with the depth. Wu (1988) and Stanton and Thornton (2000) found similar trend of void fraction distributions for the large-scale experiments and field measurements. Further, experimental results indicated that the maximum void fraction was around 20%

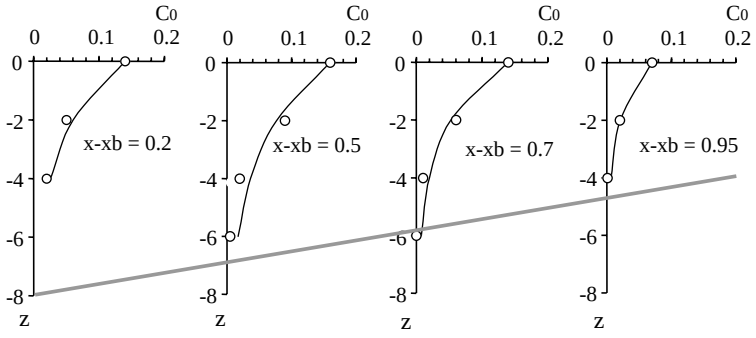

Fig. 8. Comparison of Eq. (6) with experimental data of void fractional for spilling breaker ($H_0/L_0=0.076$). The solid line (—) is from Eq. (6) and hollow symbol (○) show the experimental data.

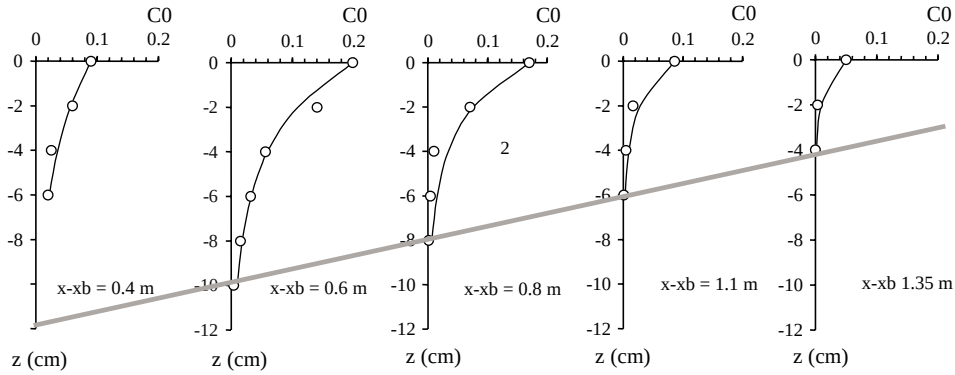

Fig. 9. Comparison of Eq. (6) with experimental data of void fractional for plunging breaker ($H_0/L_0 = 0.024$). The solid line (—) is from Eq. (6) and hollow symbol (○) show the experimental data.

near the still water level in the case of plunging breaker, whereas it was around 16% for spilling breaker. Similar results were found by Hwung et al. (1992).

5. Conclusions

The air bubbles are produced by breaking waves and then dispersed by turbulent mixing to the entire surface layer. Two parameters were used in the basic assumption of void fraction distribution and were determined by comparing with the experimental results and expressed in terms of local wave height and relative distance. The results of void fraction showed reasonable agreement between the theoretical prediction and measurements. Overall, results demonstrated that air entrainment in the surf zone is an important process by inducing a temporary water level rise and modifying the transmitted wave climate, and it cannot be ignored.

Acknowledgements

The authors would like to express special thanks to Mr Iwata for his assistance. They also acknowledge the helpful comments of Dr Hubert Chanson, Reader, University of Queensland, Australia.

References

Chanson, H., Lee, J.F., 1997. Plunging jet characteristics of plunging breakers. Coastal Eng. 31, 125–141.
Chanson, H., Aoki, S., Maruyama, M., 2002. Unsteady air bubble entrainment and detrainment at a plunging breaker: dominant time scales and similarity of water level variations. Coastal Eng. 46, 139–157.
Führböter, A., 1970. Air entrainment and energy dissipation in breakers. Proc. ICCE 1970;, 391–398.
Galvin, C.J., 1968. Breaker type classification on three laboratory beaches. J. Geophys. Res. 73 (12), 3651–3659.

Garrett, C., Li, M., Farmer, D., 2000. The connection between bubble size spectra and energy dissipation rates in the upper ocean. J. Phys. Oceanogr. 30, 2163–2171.

Hwung, H., Chyan, J., Chung, Y., 1992. Energy dissipation and air bubbles mixing inside surf zone. Proc. 23rd ICCE, ASCE 1992;, 308–321.

Iribarren, C.R., Nogales, C., 1949. Protection des ports. Section II, Comm. 4, XVIIth Int. Nav. Congress, Lisbon.

Koga, M., 1982. Bubble entrainment in breaking wind waves. Tellus 34, 481–489.

Lamarre, E., Melville, W.K., 1991. Air entrainment and dissipation in breaking waves. Nature 351, 469–472.

Loewen, M.R., Melville, W.K., 1994. An experimental investigations of the oscillations of bubble plumes entrained by breaking waves. J. Acoust. Soc. 96 (3), 1329–1343.

Stanton, T.P., Thornton, E.B., 2000. Profiles of void fraction and turbulent dissipation under breaking waves in the surf zone. Proc. 27th ICCE 1, 70–79.

Waniewski, T.A., Brennen, C.E., Raichlen, E., 2001. Measurements of air entrainment by bou waves. J. Fluids Eng. 123, 57–63.

Wu, J., 1988. Bubbles in the near-surface ocean: a general description. J. Geophys. Res. 93, 587–590.